Accepted Article Preview: Published ahead of advance online publication

This is a PDF file of an unedited peer-reviewed manuscript that has been accepted for publication. NPG is providing this early version of the manuscript as a service to our customers. The manuscript will undergo copyediting, typesetting and a proof review before it is published in its final form. Please note that during the production process errors may be discovered which could affect the content, and all legal disclaimers apply.

Sequence-defined cMET/HGFR-targeted polymers as gene delivery vehicles for the theranostic sodium iodide symporter (NIS) gene

Sarah Urnauer[1], Stephan Morys[2], Ana Krhac Levacic[2], Andrea M. Müller[1], Christina Schug[1], Kathrin A. Schmohl[1], Nathalie Schwenk[1], Christian Zach[3], Janette Carlsen[3], Peter Bartenstein[3], Ernst Wagner[2], Christine Spitzweg[1]

[1]Department of Internal Medicine II, [2]Department of Pharmacy, Center of Drug Research, Pharmaceutical Biotechnology, [3]Department of Nuclear Medicine, LMU Munich, Germany

Correspondence should be addressed to C.S. (christine.spitzweg@med.uni-muenchen.de) and E.W. (ernst.wagner@cup.uni-muenchen.de)

The laboratory work was done at the Department of Internal Medicine II and the Department of Pharmacy, LMU Munich, Germany.

Short title: Systemic non-viral NIS gene transfer

Correspondence and reprint requests:

Christine Spitzweg, Department of Internal Medicine II, University Hospital of Munich,

Marchioninistr.15, 81377 Munich, Germany; Phone: +49-89-4400-0; Fax: +49-89-4400-78737;

E-Mail: christine.spitzweg@med.uni-muenchen.de

Ernst Wagner, Department of Pharmacy, Center of Drug Research, Pharmaceutical Biotechnology, LMU Munich, Butenandstr.5-13, 81377 Munich, Germany; Phone: +49-89-2120-77840; Fax: +49-89-2120-77791;E-Mail:ernst.wagner@cup.uni-muenchen.de

ABSTRACT

The sodium iodide symporter (NIS) as well characterized theranostic gene represents an outstanding tool to target different cancer types allowing non-invasive imaging of functional NIS expression and therapeutic radioiodide application. Based on its overexpression on the surface of most cancer types, the cMET/hepatocyte growth factor receptor serves as ideal target for tumor-selective gene delivery. Sequence-defined polymers as non-viral gene delivery vehicles comprising polyethylene glycol (PEG) and cationic (oligoethanoamino) amide cores coupled with a cMET-binding peptide (cMBP2) were complexed with NIS-DNA and tested for receptor-specificity, transduction efficiency and therapeutic efficacy in hepatocellular cancer cells HuH7. *In vitro* iodide uptake studies demonstrated high transduction efficiency and cMET-specificity of NIS-encoding polyplexes (cMBP2-PEG-Stp/NIS) compared to polyplexes without targeting ligand (Ala-PEG-Stp/NIS) and without coding DNA (cMBP2-PEG-Stp/Antisense-NIS). Tumor recruitment and vector biodistribution were investigated *in vivo* in a subcutaneous xenograft mouse model showing high tumor-selective iodide accumulation in cMBP2-PEG-Stp/NIS-treated mice ($6.6 \pm 1.6\%$ ID/g ^{123}I, biological half-life 3 h) by ^{123}I-scintigraphy. Therapy studies with 3 cycles of polyplexes and ^{131}I application resulted in significant delay in tumor growth and prolonged survival. These data demonstrate the enormous potential of cMET-targeted sequence-defined polymers combined with the unique theranostic function of NIS allowing for optimized transfection efficiency while eliminating toxicity.

INTRODUCTION

As cancer is one of the leading causes of death both in developed and developing countries[1], new therapy approaches are urgently needed, especially for cancer types with poor prognosis, where surgery, chemo- and radiotherapy often prove ineffective, such as advanced hepatocellular cancer[2]. Gene therapy with its broad potential to interact and interfere with aberrant physiological processes has emerged as a powerful tool in oncology in recent years[3]. However, gene therapy still faces hurdles that strongly limit its application[4]. Low tumor selectivity of gene delivery vehicles, immunoreactions after systemic application and limited effectiveness of therapy genes have driven the search for novel biodegradable vectors with improved safety profile and enhanced transduction efficiency[5-9].

Based on its theranostic function, the sodium iodide symporter (NIS) represents an ideal therapeutic gene[9-12]. The unique combination of reporter and therapy gene characteristics allows non-invasive imaging of vector biodistribution and functional NIS expression at tumor sites by ^{123}I-scintigraphy and [124]I-/^{18}F-tetrafluoroborate positron emission tomography (PET) as well as exact dosimetric calculations before the assessment of therapeutic efficacy after application of [131]I. Several groups including our own have successfully demonstrated the capacity of NIS to induce radioiodide accumulation in different non-thyroidal tumor models mediated by various gene delivery vehicles, including mesenchymal stem cells as well as viral and non-viral vectors[13-28].

Further improvement of the NIS gene therapy concept is focused on generation of new shuttle systems with advanced efficiency, specificity and low cytotoxicity. Cationic polymers as a major sector of non-viral vectors offer the advantages of low immunogenicity, good nucleic acid binding and easy up-scaling[29]. In order to improve performance for systemic application and further enhance transduction efficiency, various design strategies have been developed for the synthesis of novel sequence-defined polymers. In this context, we generated small, well biocompatible polymer backbones with precisely

integrated functional groups. These include cationic (oligoethanoamino) amide cores for nucleic acid binding, polyethylene glycol (PEG) linkers for surface shielding, targeting ligands for cell binding and protonatable amino acids with buffer function for a higher rate of endosomal escape, leading to optimized and DNA carrier-improved systems for systemic administration[5-7].

Selective active ligand-mediated tumor-targeting represents an elegant method to further enhance tumor specificity, making use of aberrant tumor physiology that is often accompanied by up-regulation of various receptors on the surface of tumor cells, such as the epidermal growth factor receptor (EGFR)[30]. We recently reported efficient EGFR-targeting with viral and non-viral gene delivery vehicles, which resulted in high tumoral iodide uptake after systemic NIS gene transfer that was sufficient for a delay in tumor growth and prolonged survival in a subcutaneous hepatocellular cancer xenograft mouse model[14, 17]. Another attractive and important target in cancer therapy is the receptor tyrosine kinase cMET/hepatocyte growth factor receptor (HGFR). High surface expression levels and activation of cMET/HGFR in a broad range of malignancies are implicated in tumor progression and are often associated with poor prognosis[31]. In order to target non-viral gene delivery vehicles to cMET/HGFR, a cMET-binding peptide (cMBP2) was developed via phage-display screening and further identified as ideal ligand with high receptor affinity that specifically enhances nanoparticle adhesion to the target cell[7, 32-34].

In the current study, we combined the NIS gene therapy concept with novel sequence-defined polymers as non-viral gene delivery vehicles coupled to cMBP2. Based on the dual function of NIS, the potential of this cMET-targeted gene therapy approach was investigated by non-invasive imaging of vector biodistribution and transduction efficiency in a subcutaneous hepatocellular carcinoma mouse model. Subsequently, therapeutic efficacy was assessed by monitoring tumor growth after application of a therapeutic dose of ^{131}I.

RESULTS

In vitro cMET-targeted NIS-gene transfer in HuH7 and Hep3B cells

cMET/HGFR expression levels on the cell surface of HuH7 and Hep3B cells were detected by flow cytometry (**Figs. 1a,b**). High cMET/HGFR expression levels on HuH7 cells correlated well with high levels of transduction efficiency after incubation with cMET-targeted PEGylated polyplexes cMBP2-PEG-Stp/NIS (Stp=succinoyl-tetraethylene pentamine), while significantly lower transgene expression levels were obtained after transfection of low cMET/HGFR expressing Hep3B cells (**Fig. 1c**). This led to the selection of the HuH7 cell line as model system for further *in vitro* and *in vivo* experiments. Transduction conditions were optimized by measurement of perchlorate-sensitive iodide uptake activity 24 h after NIS gene transfer and best conditions with lowest cytotoxicity were used in all subsequent experiments. Incubation of HuH7 cells with cMBP2-PEG-Stp/NIS polyplexes resulted in a 12-fold increase in ^{125}I uptake compared to empty polymers, which was completely blocked upon treatment with the NIS-specific inhibitor sodium perchlorate. In contrast, replacement of the targeting ligand cMBP2 by alanine (Ala-PEG-Stp/NIS) showed a significantly lower iodide uptake activity, demonstrating targeting specificity of the targeting ligand cMBP2. No iodide uptake above background levels was seen in HuH7 cells transfected with empty polymers cMBP2-PEG-Stp and cMBP2-PEG-Stp/Antisense-NIS (**Fig. 1d**). Results were normalized to cell viability. Cell viability was not affected by polyplex-mediated gene transfer (**Fig. 1e**).

In vivo iodide uptake studies after systemic NIS gene transfer

To evaluate vector biodistribution and functional NIS expression after cMET-targeted gene transfer in HuH7 tumor-bearing mice, animals received an intraperitoneal dose of ^{123}I 24 h or 48 h after intravenous application of polyplexes. Radioiodide biodistribution was assessed by gamma camera imaging and

regions of interest were quantified. A considerably higher tumoral iodide uptake was observed in tumors of mice that received ^{123}I 48 h after application of cMBP2-PEG-Stp/NIS polyplexes as compared to 24 h (data not shown). For all subsequent *in vivo* experiments, radionuclide application was conducted 48 h after polyplex administration.

In contrast to high levels of radionuclide accumulation in 80% (7 out of 9) of tumors of mice treated with cMBP2-PEG-Stp/NIS **(Fig. 2a)**, tumors of mice injected with the untargeted control polyplex Ala-PEG-Stp/NIS exhibited only weak tumoral iodide accumulation **(Fig. 2b)**. No tumoral iodide uptake above background levels was measured after treatment with cMBP2-PEG-Stp/Antisense-NIS polyplexes **(Fig. 2c)**. Physiological expression of NIS in thyroid and stomach resulted in iodide accumulation in theses tissues and, due to renal elimination of radioiodide, iodide uptake was also observed in the bladder. No additional iodide uptake was recorded in non-targeted organs such as lung, liver, kidney and spleen. NIS-specificity was confirmed by intraperitoneal application of the NIS-specific inhibitor sodium perchlorate 30 min prior to radionuclide application, which resulted in an almost complete inhibition of iodide uptake in the tumor and organs that physiologically express NIS **(Fig. 2d)**. Serial scanning revealed a maximal ^{123}I accumulation of 6.6±1.6% ID/g (percentage of the injected dose per gram tumor) in NIS-transduced HuH7 xenografts with a biological half-life of 3 h **(Fig. 2e)**. A tumor-absorbed dose of 41 mGy/MBq/g tumor with an effective half-life of 3 h for ^{131}I was calculated.

Ex vivo biodistribution studies after systemic NIS gene transfer

Ex vivo biodistribution was performed to further assess tumor-specific iodide uptake after systemic polyplex administration. 3 h after ^{123}I application, mice were sacrificed, organs dissected and subsequently measured in a gamma counter. *Ex vivo* biodistribution results correlated well with gamma imaging results, showing a perchlorate-sensitive tumoral radioiodide uptake of 3% of the injected dose per organ in cMBP2-PEG-Stp/NIS-treated mice 3 h after injection of the radionuclide. Moreover, almost

no iodide uptake was detected in non-target organs and tumors of control mice that received either Ala-PEG-Stp/NIS, cMBP2-PEG-Stp/Antisense-NIS or cMBP2-PEG-Stp/NIS and sodium perchlorate (**Fig. 2f**).

Immunohistochemical analysis of NIS protein expression after polyplex-mediated gene transfer

Immunohistochemical analysis of NIS protein expression in HuH7 xenografts 48 h after cMET-targeted polyplex-mediated gene transfer revealed a heterogeneous staining pattern with multiple clusters of NIS-specific immunoreactivity in tumors of mice that received cMBP2-PEG-Stp/NIS (**Figs. 3a,b**). In both control groups (Ala-PEG-Stp/NIS, cMBP2-PEG-Stp/Antisense-NIS) no specific NIS expression was detected (**Figs. 3c,d**), which is comparable to untreated tumor tissue (**Fig. 3e**).

Quantification of *NIS* mRNA expression by quantitative real-time PCR analysis

To determine *NIS* mRNA levels in HuH7 xenograft, mRNA was analyzed by quantitative real-time PCR (qPCR) 48 h after systemic NIS gene transfer (**Fig. 3f**). High levels of *NIS* gene expression were measured in tumors of cMBP2-PEG-Stp/NIS-treated mice and tumors of mice that received the NIS-specific inhibitor sodium perchlorate before administration of cMBP2-PEG-Stp/NIS. Lower *NIS* expression levels were observed in tumors of mice treated with Ala-PEG-Stp/NIS. No *NIS* expression above background levels were seen in cMBP2-PEG-Stp/Antisense-NIS-treated mice.

Radioiodide therapy studies after cMET-targeted non-viral NIS gene delivery

Therapeutic efficacy was evaluated after establishment of an optimal time scheme of repetitive polyplex and ^{131}I application. Mice received either cMBP2-PEG-Stp/NIS, Ala-PEG-Stp/NIS or cMBP2-PEG-

Stp/Antisense-NIS followed by a therapeutic dose of 55.5 MBq ^{131}I or cMBP2-PEG-Stp/NIS followed by saline 48 h later. The cycle of gene transfer and radioiodine application was conducted three times on days 0/2, 3/5 and 7/9. Mice treated with cMBP2-PEG-Stp/NIS that received radioiodide showed a significant delay in tumor growth as compared to all control groups **(Fig. 4a)**. This was associated with markedly improved survival **(Fig. 4b)**. While mice of control groups had to be sacrificed within 3-4 weeks after onset of the therapy trial due to excessive tumor growth, mice treated with cMBP2-PEG-Stp/NIS and ^{131}I survived up to nearly 7 weeks.

Immunofluorescence analysis

After therapy, at the end of the observation period, mice were sacrificed, tumors dissected and tissues further processed for immunofluorescence analysis. A Ki67-specific antibody (green) was used to determine cell proliferation and an antibody against CD31 (red) labeled blood vessels **(Figs. 5a-d)**. Tumors of animals treated with cMBP2-PEG-Stp/NIS that received ^{131}I, exhibited a significantly decreased proliferation and lower blood vessel density as compared to control groups (cMBP2-PEG-Stp/NIS+NaCl; cMBP2-PEG-Stp/Antisense-NIS+^{131}I; Ala-PEG-Stp/NIS+^{131}I) **(Figs. 5e,f)**.

DISCUSSION

Gene therapy is emerging as a highly promising approach to disrupt cancer homeostasis through replacement or silencing of malfunctioning genes and insertion of new genes that directly kill cancer cells[35, 36]. In this context, NIS represents an ideal candidate gene for therapeutic intervention. Its unique capacity to act both as reporter and therapy gene allows us to monitor biodistribution of functional NIS expression by multimodal nuclear medicine imaging modalities and at the same time allows application of a therapeutic dose of ^{131}I[9, 12, 37-40]. Currently, the NIS gene therapy concept is being evaluated in

prostate cancer patients after local adenovirus-mediated NIS gene delivery (NCT00788307)[41, 42]. Moreover, the reporter function of NIS is being tested in various protocols in different cancer types, including head, neck, ovarian and peritoneal cancer to monitor biodistribution of genetically engineered oncolytic measles virus and mesenchymal stem cells that express NIS[43-47]. However, systemic application with its potential to target metastatic disease requires further improvement of shuttle systems, as the potential of therapeutic genes is highly dependent on efficient and tumor-selective delivery. The delivery pathway from injection site to distant tumor sites poses several major obstacles that need to be overcome[48, 49]. Besides nuclease-dependent stability of nucleic acids in blood circulation, stable complexes of nucleic acid and vector system need to be formed to achieve long-term persistence of systemically applied delivery vehicles. Further requirements include an enhanced safety profile for reduced interactions with blood components and low immunogenicity as well as high targeting specificity to minimize effects on non-target cells and to achieve sufficiently high gene expression levels specifically in tumor tissue. Additionally, after entering the target cell via endocytic cellular uptake, protection from lysosomal degradation along with efficient endosomal escape are crucial steps for intracellular delivery of genetic information[29, 48, 49].

In our previous preclinical studies, we investigated the potential of viral and non-viral vector systems to deliver the NIS gene to non-thyroidal tumor cells after systemic application[13-23, 37, 50-52]. Viral vectors represent a highly efficient option due to their inherent capacity to insert their genetic material into host cells, as we have shown using different adenoviral vectors[13-15, 19, 52]. However, these vectors bear a series of limitations including high immunogenicity, unspecific cell tropism and uncontrolled insertion of DNA into the host genome[29, 53]. We further demonstrated the feasibility of non-viral delivery vehicles based on biodegradable pseudodendritic oligoamines and EGFR-targeted LPEI-PEG-polymers. Application of pseudodendritic polymers G2-HD-OEI in different tumor models led to high NIS-mediated tumoral iodide accumulation and subsequently high therapeutic efficiency. As there is no specific targeting ligand, tumor selectivity was mostly obtained by high intrinsic tumor affinity through

the so-called "enhanced permeability and retention" effect in these well-vascularized tumors with leaky blood vessel structure[16, 18, 54]. Active EGF-receptor targeting of LPEI-PEG-GE11 polymers via the GE11 ligand resulted in high specific iodide accumulation in tumor tissue. Receptor mediated uptake could be confirmed by pretreatment with the EGFR-specific antibody cetuximab showing significant decrease of polyplex uptake in tumor cells and NIS expression[17]. However, the main drawbacks of these non-viral delivery systems are the variable constitution and polydispersity as well as limited specificity of untargeted pseudodendritic oligoamines and the low biocompatibility and long-term toxicity of LPEI-derivatives. Consequently, for clinical application of synthetic non-viral gene delivery vehicles, it is indispensable to develop highly defined substances with improved efficiency, low immunogenicity and a precise, constant and easily reproducible structure.

These desirable features can be realized through the design of novel sequence-defined polymers with structure-activity relationships by solid-phase synthesis[55], allowing generation of precise backbones and incorporation of multiple functional groups. The optimal balance between the formation of stable polyplexes and efficient release of DNA at the target site is obtained by serial synthesis of artificial amino acid succinoyl-tetraethylenepentamine (Stp) repeats which contain a diaminoethane motif and form the basic polymer structure[6, 7]. This functional site exhibits optimal DNA condensation ability, equips the polymer with buffering amine functions and shows enhanced biodegradability and low toxicity compared to the "gold standard" LPEI. Terminal cysteines further support polyplex stabilization via disulfide bridges. For surface shielding, hydrophilic PEG domains are incorporated that reduce non-specific interactions with serum components, thus leading to a higher safety profile and lower immunogenicity of polyplexes. Additional histidines as protonatable amino acids with high buffering capacity are integrated to improve endosomal escape for adequate release of polymers in target cells[7, 56]. Active ligand-mediated targeting is an elegant method to enhance tumor specificity and thus amplify transgene expression in tumoral tissues while reducing side effects in non-target organs[49]. Active targeting is a prerequisite for clinical application, as polymer accumulation in tumor tissue by passive

targeting is highly dependent on retention effects and leaky vascular structure[57, 58]. As growth factor receptors are often overexpressed and play a crucial role in tumor progression, promising candidates that act as ligands have been developed via phage display analysis with a focus on short peptides, as they are easy to synthesize and show high receptor affinity. In previous studies, we have already shown the efficacy of the short peptide GE11 for EGFR targeting[14, 17]. Another attractive target receptor in cancer therapy is cMET/HGFR. High surface expression levels and activation of cMET in a broad range of malignancies are implicated in tumor progression and metastasis and are often associated with poor prognosis[31]. The cMET-binding peptide cMBP2 was identified as an ideal ligand with high receptor affinity that specifically enhances nanoparticle adhesion to the target cell without activating the receptor[7, 32, 33]. Peptide ligand specificity was confirmed by high cell binding of cMBP2-polyplexes to cMET/HGFR over-expressing prostate cancer cells DU145[7] and HCC cells HuH7, in contrast to alanine ligand control and four different scrambled sequences of cMBP2 which showed no specific cellular binding[6]. Furthermore, a novel flow method to assess the potential of peptides to specifically bind to their receptors demonstrated sequence-specificity of cMBP2 in binding to the cMET/HGFR expressing HuH7 HCC cell line[32]. Therefore, in this study, we selected cMBP2 as ligand for our innovative sequence-defined cMET-targeted polymers to direct NIS expression to HuH7 HCC xenograft mouse model. The HCC cell line HuH7 represents an attractive platform for cMET-targeted non-viral gene delivery due to its high levels of endogenous surface expression of cMET/HGFR.

High levels of natural cMET expression on HuH7 cells were confirmed via flow cytometry analysis and expression levels were shown to correlate well with *in vitro* transfection efficiency of cMET-targeted polyplexes cMBP2-PEG-Stp/NIS in comparison with the low cMET expressing HCC cell line Hep3B . Further *in vitro* transfection studies using high cMET/HGFR-expressing HuH7 cells revealed an ideal ratio of 12 protonatable nitrogen groups in the polymer backbone per negatively charged phosphate in the nucleic acid (N/P), which resulted in optimal nucleic acid binding, very low toxicity and highest

transfection levels. To optimize particle size and DNA compaction for subsequent *in vivo* application, the three-armed non-PEGylated polymer #689 (3-arm-Stp) was added at 30 molar percentage.

As a next step, we took further advantage of the reporter function of NIS to investigate transduction efficiency of cMET-targeted polyplexes *in vivo*.[123]I gamma camera imaging of vector biodistribution and functional NIS expression in HuH7 tumor-bearing mice revealed a high tumor-specific iodide uptake of 6.6±1.6% ID/g in cMBP2-Stp-PEG/NIS-treated mice 48 h after intravenous polyplex administration. Significantly lower tumoral iodide accumulation after injection of Ala-PEG-Stp/NIS polyplexes verified improved tumor-selective transduction efficiency of actively targeted polyplexes. The significantly lower, but measureable iodide uptake after transfection with untargeted Ala-PEG-Stp/NIS polyplexes is due to basal transduction efficiency of the untargeted polymer based on passive targeting effects through the so-called "enhanced permeability and retention" effect in well-vascularized tumors[16, 18, 54]. The significant differences in ^{123}I uptake of cMET-targeted polyplexes in comparison to untargeted polyplexes *in vivo* underline the remarkable targeting-effects of the cMBP2 ligand. Pretreatment with the NIS-specific inhibitor sodium perchlorate in a subgroup of cMBP2-PEG-Stp/NIS-treated mice as well as an additional control group treated with cMBP2-PEG-Stp/Antisense-NIS polyplexes led to comparably low iodide uptake demonstrating NIS-specificity. Data obtained by *ex vivo* biodistribution correlated well with results from gamma camera imaging, showing a tumoral iodide accumulation of 3.0±0.5% ID/organ in cMBP2-PEG-Stp/NIS-treated mice 3 h post ^{123}I application. In addition, no specific iodide accumulation was observed in tumors of control mice and non-target organs, confirming tumor specificity of gene delivery vehicles based on active cMET-targeting. These results clearly demonstrate targeting specificity of cMBP2 as cMET-binding peptide and the efficacy of our novel sequence defined polymers as gene delivery vehicles.

After successfully demonstrating the feasibility of this polyplex-mediated NIS gene therapy approach *in vitro* and *in vivo* taking advantage of NIS in its function as reporter gene, we addressed the question whether tumor-specific transduction is sufficiently high for a therapeutic effect. After three cycles of

repetitive polyplex and radioiodide application, a significant reduction in tumor growth was observed in mice treated with cMBP2-PEG-Stp/NIS. This was associated with a prolonged survival of up to nearly 7 weeks, whereas animals of control groups had to be sacrificed within 3-4 weeks. Immunohistochemical staining revealed a heterogenous staining pattern with clusters of membrane associated NIS-specific immunoreactivity. As NIS gene therapy is associated with a high bystander effect based on the crossfire effect of the beta-emitter ^{131}I, the cytotoxic effect is not only limited to transduced cells, but also affects surrounding cells increasing therapeutic effectiveness of the NIS gene therapy concept. These findings were confirmed by immunofluorescence analysis of tumors after treatment: tumors from animals treated with cMBP2-PEG-Stp/NIS exhibited reduced cell proliferation and blood vessel density as compared to all control groups. As the immunofluorescence analysis experiments were performed at the end of the observation period, i.e. at different time points in the control group vs. therapy group, in which mice were sacrificed at a later stage, other factors such as mouse age, might influence the results. However, as mice were sacrificed in the therapy group when significant regrowth of tumors had occurred, our results probably even underestimate the antiproliferative and antiangiogenic effects of ^{131}I therapy following cMBP2-PEG-Stp/NIS-mediated NIS gene transfer.

In our studies, a therapeutic dose of 55.5 MBq [131]I (1.5 mCi) was used[13-20, 52] based on initial tests on radiation safety, tolerability and efficacy[13, 52]. The Food and Drug Administration of the United States (FDA) formulated a table of dose conversion factors that allows for allometric adaption from preclinical animal models to humans based on body surface area (BSA)[59]. Using this method, the mouse dose of 55.5 MBq translates to 13.9 GBq (372 mCi) for a 75kg human being, which lies within the dosimetrically determined dose range (300 mCi – 600 mCi) in patients with advanced metastasized differentiated thyroid cancer[60]. In order to keep potential toxicities at a minimum, the calculated dose should not represent a fixed applicable dose, but a dose range that needs to be adjusted in a personalized manner considering various factors including the radiation sensitivity of the tumor, co-morbidities of the patient and pretreatments. In this context, the concept of the theranostic application of the NIS gene

allows optimal adjustment of the ^{131}I dose based on exact dosimetric calculations of doses to the tumor and other organs from radioiodine imaging studies to limit side effects to non-target organs including bone marrow, spinal cord, salivary glands, upper gastrointestinal tract, kidneys and bladder.

Based on these promising preclinical results, the next crucial step towards clinical application will be a toxicity study, specifically designed to assess potential toxicities arising from cMBP2-PEG-Stp/NIS application followed by saline or ^{131}I application. For this purpose, naive mice without tumor will be used, cMBP2-PEG-Stp/NIS will be injected i.v. as well as directly into critical organs such as the liver and lungs, followed by assessment of toxicity by physical examination, blood and tissue sampling at early, intermediate and late time points (such as 1 week up to 3 months).

Our data clearly demonstrate the therapeutic efficacy of cMET-targeted NIS gene therapy. Combined with our previous results targeting NIS to EGFR on tumor cells using the peptide GE11, this opens the exciting prospect of a possible future combination of these two targeting agents. The concept of dual targeting mimicks the natural process of viral cellular uptake, as several viruses, including adenoviruses, target two receptor types for so-called biphasic cell entry. The synergistic effects of targeting the receptors for EGF and transferrin using synthetic polymers have already been explored *in vitro*[6]. Studies postulating crosstalk between EGFR and cMET on cancer cells further substantiate the potential of dual targeting of these two receptors, especially as cMET amplification has been implicated in resistance mechanisms to escape EGFR-targeted therapy[61-64].

In conclusion, our data demonstrate the enormous potential of sequence-defined polymers for cMET-targeted NIS gene delivery. The precise synthesis of these novel polymers allows for optimized transfection efficiency while eliminating adverse effects such as toxicity or high immunogenicity. High cMET expression levels on many cancer cells make this receptor an ideal target in cancer therapy. Combined with the unique theranostic function of NIS, our targeting strategy led to significant tumoral iodide uptake that was sufficient for potent therapeutic effects after ^{131}I application. This innovative concept of active receptor-targeted non-viral gene delivery is of high clinical relevance as it optimizes

efficacy and safety of systemic NIS gene delivery and opens the exciting prospect of application in metastatic disease.

MATERIALS AND METHODS

Cell culture

The human hepatocellular carcinoma cell line HuH7 (JCRB0403; Japanese Collection of Research Bioresources Cell Bank, Osaka, Japan) was cultured in Dulbecco's modified eagle medium (DMEM; 1 g/l glucose; Sigma-Aldrich, St.Louis, Missouri, USA) and the human hepatocellular carcinoma cell line Hep3B (HB-8064; American Type Culture Collection (ATCC), Manassas, VA) was cultured in Eagle's Minimum Essential Medium (EMEM; Sigma-Aldrich). Both media were supplemented with 10% (v/v) fetal bovine serum (FBS Superior, Biochrom/Merck Milipore, Berlin, Germany) and 1% (v/v) penicillin/streptomycin (Sigma-Aldrich).

Cells were maintained at 37°C and 5% CO_2 in an incubator with a relative humidity of 95%. Cell culture medium was replaced every second day and cells were passaged at 80% confluency.

Plasmid and polymer synthesis

The expression vector pCpG-hCMV-NIS driven by the human elongation factor 1α promotor and human cytomegalovirus enhancer element containing the full-length codon-optimized *NIS* cDNA (Geneart, Regensburg, Germany) was generated as described previously[17]. For all *in vitro* and *in vivo* experiments pNIS-DNA produced and purified by Plasmid Factory GmbH (Bielefeld, Germany) was used. Synthesis of polymers was carried out as described previously[7] and polymers were used as 5 mg/ml stock solutions.

Polyplex formation

For polyplex formation the sequence-defined histidinylated cMET-targeted polymer (cMBP2-PEG-Stp) or a control polymer with alanine instead of the ligand (Ala-PEG-Stp) and a PEG-free three-armed polymer (3-arm-Stp, #689) in a molar ratio of 70:30 to compact polyplexes were used[7]. The polymer blend and plasmid DNA (pDNA) were diluted in same volumes of HEPES buffered glucose (HBG: 20 mmol/l HEPES, 5% glucose (w/v) at pH 7.4). Polymers were added to the DNA by rapid mixing at a N/P (nitrogen/phosphate) ratio (w/w) of 12 and incubated at room temperature for 30 minutes before use. For calculation, only protonatable nitrogen groups were considered. Final DNA concentration for *in vitro* studies was 2 µg/ml, for *in vivo* studies 200 µg/ml.

Transient transfection and ^{125}I uptake assay

To measure the transduction efficiency, cells were grown to 60-80% confluency (2×10^5 HuH7 or Hep3B cells/well in 6-well-plates) and incubated for 4 hours with DNA/polymer-solutions in serum- and antibiotic-free medium. Medium was then changed to normal growth medium and, 24 h later, iodide uptake activity was measured. NIS-mediated ^{125}I uptake assays were performed as described previously[23]. Results were normalized to cell survival measured by cell viability assay (see below) and expressed as cpm/A620.

Cell viability assay

Cells were incubated with a commercially available MTT reagent (Sigma-Aldrich) for 2 h at 37°C followed by a washing step with PBS (phosphate-buffered saline). Cell viability was measured after

incubation with 10% DMSO (dimethyl sulfoxide) in isopropanol at 620 nm in a Sunrise microplate absorbance reader (Tecan, Männedorf, Switzerland).

Flow cytometry analysis

Cell surface cMET/HGF-receptor expression levels were quantified by flow cytometry analysis. HuH7-cells and Hep3B cells were detached with trypsin and washed with FACS buffer (PBS with 10% FBS). Cells were incubated with an antibody that detects human cMET/HGFR (1:200; monoclonal mouse IgG1, R&D Systems, Minneapolis, USA) for 1 h on ice. As negative control, an IgG-anti-mouse antibody (BD Bioscience, Franklin Lakes, USA) was used. After incubation, cells were washed with FACS-buffer, stained with an AlexaFluor 488-labeled goat anti-mouse secondary antibody (1:400; Jackson ImmunoResearch, West Grove, Pennsylvania, USA) for 1 h on ice, washed and resuspended in FACS buffer. Analysis was performed on a BD Accuri[TM] C6 flow cytometer (BD Bioscience, Franklin Lakes, USA). Cells were gated by forward/sideward scatter and pulse width for exclusion of doublets. PI (propidium iodine, Sigma-Aldrich) was used for discrimination between viable and dead cells.

Establishment of subcutaneous HuH7 tumors

HuH7 xenografts were established in 6-week-old female CD-1 nu/nu mice (Charles River, Sulzfeld, Germany) by subcutaneous injection of 5×10^6 HuH7 cells suspended in 100 µl of PBS into the flank region. Animals were maintained under specific pathogen-free conditions with access to mouse chow and water *ad libitum*. Before radionuclide application, mice were pretreated with L-T4 (L-thyroxine, 5 mg/l; Sigma-Aldrich) in drinking water to reduce iodide uptake in the thyroid gland.

Tumor measurements were performed regularly and tumor volume was estimated using the equation: length x width x height x 0.52. Animals were sacrificed when the tumor volume reached a size of

1500 mm^3 or tumors necrotized. The experimental protocol was approved by the regional governmental commission for animals (Regierung von Oberbayern) and all animal experiments were carried out according to the guidelines of the German law of protection of animal life.

In vivo radioiodide imaging and biodistribution studies after NIS gene transfer

When subcutaneous HuH7 tumors reached a size of 10-15 mm in diameter, polyplex solutions containing 50 μg of pNIS-DNA were applied via the tail vein. Animals were divided into three groups and treated either with cMBP2-PEG-Stp/NIS (n=15), cMBP2-PEG-Stp/Antisense-NIS (n=5) or Ala-PEG-Stp/NIS (n=5). 48 hours after polyplex administration, mice received an intraperitoneal injection of 18.5 MBq ^{123}I. To determine NIS specificity, a subgroup of cMBP2-PEG-Stp/NIS-treated mice received NaClO$_4$ (sodium perchlorate; 2 mg/mouse; Sigma-Aldrich), a NIS-specific inhibitor, 30 min prior to radioiodide application (n=6). Vector biodistribution and tumoral NIS expression were determined by measuring the iodide uptake by serial gamma camera imaging (e.cam, Siemens, Munich, Germany; with a low-energy high resolution collimator). Regions of interest were quantified by using the software HERMES GOLD (Hermes Medical Solutions, Stockholm, Sweden) and are shown as percent of injected iodide dose per gram tumor tissue (% ID/g).

Ex vivo biodistribution studies

For *ex vivo* biodistribution studies, mice of the cMBP2-PEG-Stp/NIS group (n=6), cMBP2-PEG-Stp/NIS+NaClO$_4$ (n=3) group, cMBP2-PEG-Stp/Antisense-NIS group (n=3) or Ala-PEG-Stp/NIS group (n=3) received 18.5 MBq ^{123}I to detect iodide accumulation in the tumor and non-target organs. 3 h after injection of ^{123}I, mice were sacrificed and organs were dissected and

measured in a Packard Cobra Quantum Gamma Counter (GMI, Ramsey, Minnesota, USA). Results are presented as percent injected dose per organ (% ID/organ).

Immunohistochemical NIS staining

Immunohistochemical NIS staining was performed on dissected frozen tissues of HuH7 tumors 48 h after systemic administration of polyplexes. A NIS specific mouse monoclonal antibody (Millipore, Darmstadt, Germany; 1:1000) was used for NIS detection and staining was performed as described previously[65] Sections were imaged on an Olympus BX41 microscope (Olympus, Shimjukum Tokio, Japan) equipped with an Olympus XC30 CCD camera (Olympus).

Radioiodide therapy study *in vivo*

Therapy studies started when subcutaneous HuH7 tumors reached a size of 5-6 mm. Three cycles of polyplex administration were performed on day 0, 3 and 7. Mice received either cMBP2-PEG-Stp/NIS (n=10), cMBP2-PEG-Stp/Antisense-NIS (n=6) or Ala-PEG-Stp/NIS (n=6) followed by an intraperitoneal application of 55.5 MBq ^{131}I 48 h later. As additional controls mice received cMBP2-PEG-Stp/NIS followed by saline (NaCl; n=9). Mouse survival was defined by a maximum tumor volume of 1500 mm^3 at which animals had to be sacrificed.

Analysis of NIS mRNA expression

For quantification of NIS expression, total RNA was isolated from HuH7 tumors using the RNeasy Mini Kit (Quiagen, Hilden, Germany) according to the manufacturer's recommendations. Reverse transcription was performed using SuperScript III First-Strand Synthesis System (Thermo Fisher

Scientific, Waltham, Massachusetts, USA). Quantitative real-time PCR was run with the QuantiTect SYBR Green PCR Kit (Qiagen) in a Mastercycler ep gradient S PCR cycler (Eppendorf, Hamburg, Germany). Relative expression levels were calculated from ΔΔCt values normalised to internal β-actin. The following primers were used:

hNIS: (5'ACACCTTCTGGACCTTCGTG-3') and (5'-GTCGCAGTCGGTGTAGAACA-3'),

β-Actin: (5'AGAAAATCTGGCACCACACC-3') and (5'-TAGCACAGCCTGGATAGCAA-3')

Indirect immunofluorescense assay

After treatment, at the end of the observation period, immunofluorescence staining was performed on dissected frozen tissues, which were fixed in 80% methanol at 4°C for 5 min and acetone at -20°C for 2 min. After rehydration in PBS and blocking with 12% bovine serum albumin/PBS for 30 min at room temperature, incubation with a rabbit polyclonal antibody against human Ki67 (Abcam, Cambridge, UK; dilution 1:1000) and a rat monoclonal antibody against mouse CD31 (BD Pharmingen, Heidelberg, Germany; dilution 1:200) was performed. This was followed by incubation with a secondary anti-rabbit Alexa488-conjugated antibody (Jackson ImmunoResearch, West Grove, Pennsylvania, USA) for Ki67 staining and secondary anti-rat Cy3-conjugated antibody (Jackson ImmunoResearch) for CD31 staining. Nuclei were counterstained with Hoechst bisbenzimide (5 mg/ml) and sections were embedded in Fluorescent Mounting Medium (Dako, Hamburg, Germany). Stained sections were examined using an Axiovert 135 TV fluorescence microscope equipped with an AxioCam MRm CCD camera and AxioVision Re. 4.8. software (Carl Zeiss, Munich, Germany). Quantification of proliferation (Ki67-staining) and blood vessel density (CD31-staining) was performed by evaluation of 6 visual fields per tumor using ImageJ software (NIH).

Statistical methods

All *in vitro* experiments were carried out at least in triplicates. Results are expressed as mean ± SEM, mean fold change ± SEM and, for survival plots, in percent. Statistical significance was calculated by two-tailed Student's t-test for *in vitro* and *ex vivo* experiments or Mann-Whitney U test for *in vivo* experiments. *P* values ≤0.05 were considered significant (*p≤0.05, **p≤0.01, ***p≤0.001).

REFERENCES

1. Fitzmaurice, C, Dicker, D, Pain, A, Hamavid, H, Moradi-Lakeh, M, MacIntyre, MF, *et al.* (2015). The Global Burden of Cancer 2013. *JAMA oncology* **1**: 505-527.

2. Davis, GL, Dempster, J, Meler, JD, Orr, DW, Walberg, MW, Brown, B, *et al.* (2008). Hepatocellular carcinoma: management of an increasingly common problem. *Proceedings (Baylor University Medical Center)* **21**: 266-280.

3. Amer, MH (2014). Gene therapy for cancer: present status and future perspective. *Molecular and cellular therapies* **2**: 27.

4. Akinc, A, Thomas, M, Klibanov, AM, and Langer, R (2005). Exploring polyethylenimine-mediated DNA transfection and the proton sponge hypothesis. *The journal of gene medicine* **7**: 657-663.

5. He, D, and Wagner, E (2015). Defined polymeric materials for gene delivery. *Macromolecular bioscience* **15**: 600-612.

6. Kos, P, Lachelt, U, He, D, Nie, Y, Gu, Z, and Wagner, E (2015). Dual-targeted polyplexes based on sequence-defined peptide-PEG-oligoamino amides. *J Pharm Sci* **104**: 464-475.

7. Kos, P, Lachelt, U, Herrmann, A, Mickler, FM, Doblinger, M, He, D, *et al.* (2015). Histidine-rich stabilized polyplexes for cMet-directed tumor-targeted gene transfer. *Nanoscale* **7**: 5350-5362.

8. Roder, R, and Wagner, E (2014). Sequence-defined shuttles for targeted nucleic acid and protein delivery. *Therapeutic delivery* **5**: 1025-1045.

9. Hingorani, M, Spitzweg, C, Vassaux, G, Newbold, K, Melcher, A, Pandha, H, *et al.* (2010). The biology of the sodium iodide symporter and its potential for targeted gene delivery. *Current cancer drug targets* **10**: 242-267.

10. Harrington, KJ, Spitzweg, C, Bateman, AR, Morris, JC, and Vile, RG (2001). GENE THERAPY FOR PROSTATE CANCER: CURRENT STATUS AND FUTURE PROSPECTS. *The Journal of Urology* **166**: 1220-1233.

11. Christine Spitzweg, JCM (2002). The sodium iodide symporter: its pathophysiological and therapeutic implications. vol. 57. pp 559-574.

12. Spitzweg, C, Harrington, KJ, Pinke, LA, Vile, RG, and Morris, JC (2001). The Sodium Iodide Symporter and Its Potential Role in Cancer Therapy. vol. 86. pp 3327-3335.

13. Grunwald, GK, Klutz, K, Willhauck, MJ, Schwenk, N, Senekowitsch-Schmidtke, R, Schwaiger, M*, et al.* (2013). Sodium iodide symporter (NIS)-mediated radiovirotherapy of hepatocellular cancer using a conditionally replicating adenovirus. *Gene therapy* **20**: 625-633.

14. Grunwald, GK, Vetter, A, Klutz, K, Willhauck, MJ, Schwenk, N, Senekowitsch-Schmidtke, R*, et al.* (2013). EGFR-Targeted Adenovirus Dendrimer Coating for Improved Systemic Delivery of the Theranostic NIS Gene. *Mol Ther Nucleic Acids* **2**: e131.

15. Grunwald, GK, Vetter, A, Klutz, K, Willhauck, MJ, Schwenk, N, Senekowitsch-Schmidtke, R*, et al.* (2013). Systemic image-guided liver cancer radiovirotherapy using dendrimer-coated adenovirus encoding the sodium iodide symporter as theranostic gene. *Journal of nuclear medicine : official publication, Society of Nuclear Medicine* **54**: 1450-1457.

16. Klutz, K, Russ, V, Willhauck, MJ, Wunderlich, N, Zach, C, Gildehaus, FJ*, et al.* (2009). Targeted radioiodine therapy of neuroblastoma tumors following systemic nonviral delivery of the sodium iodide symporter gene. *Clinical cancer research : an official journal of the American Association for Cancer Research* **15**: 6079-6086.

17. Klutz, K, Schaffert, D, Willhauck, MJ, Grunwald, GK, Haase, R, Wunderlich, N*, et al.* (2011). Epidermal growth factor receptor-targeted (131)I-therapy of liver cancer following systemic delivery of the sodium iodide symporter gene. *Molecular therapy : the journal of the American Society of Gene Therapy* **19**: 676-685.

18.   Klutz, K, Willhauck, MJ, Dohmen, C, Wunderlich, N, Knoop, K, Zach, C, *et al.* (2011). Image-guided tumor-selective radioiodine therapy of liver cancer after systemic nonviral delivery of the sodium iodide symporter gene. *Human gene therapy* **22**: 1563-1574.

19.   Klutz, K, Willhauck, MJ, Wunderlich, N, Zach, C, Anton, M, Senekowitsch-Schmidtke, R*, et al.* (2011). Sodium iodide symporter (NIS)-mediated radionuclide ((131)I, (188)Re) therapy of liver cancer after transcriptionally targeted intratumoral in vivo NIS gene delivery. *Human gene therapy* **22**: 1403-1412.

20.   Knoop, K, Kolokythas, M, Klutz, K, Willhauck, MJ, Wunderlich, N, Draganovici, D*, et al.* (2011). Image-guided, tumor stroma-targeted 131I therapy of hepatocellular cancer after systemic mesenchymal stem cell-mediated NIS gene delivery. *Molecular therapy : the journal of the American Society of Gene Therapy* **19**: 1704-1713.

21.   Knoop, K, Schwenk, N, Dolp, P, Willhauck, MJ, Zischek, C, Zach, C*, et al.* (2013). Stromal targeting of sodium iodide symporter using mesenchymal stem cells allows enhanced imaging and therapy of hepatocellular carcinoma. *Human gene therapy* **24**: 306-316.

22.   Knoop, K, Schwenk, N, Schmohl, K, Muller, A, Zach, C, Cyran, C*, et al.* (2015). Mesenchymal stem cell-mediated, tumor stroma-targeted radioiodine therapy of metastatic colon cancer using the sodium iodide symporter as theranostic gene. *Journal of nuclear medicine : official publication, Society of Nuclear Medicine* **56**: 600-606.

23.   Spitzweg, C, Zhang, S, Bergert, ER, Castro, MR, McIver, B, Heufelder, AE*, et al.* (1999). Prostate-specific antigen (PSA) promoter-driven androgen-inducible expression of sodium iodide symporter in prostate cancer cell lines. *Cancer research* **59**: 2136-2141.

24.   Spitzweg, C, O'Connor, MK, Bergert, ER, Tindall, DJ, Young, CY, and Morris, JC (2000). Treatment of prostate cancer by radioiodine therapy after tissue-specific expression of the sodium iodide symporter. *Cancer research* **60**: 6526-6530.

25. Miller, A, and Russell, SJ (2016). The use of the NIS reporter gene for optimizing oncolytic virotherapy. *Expert opinion on biological therapy* **16**: 15-32.

26. Oneal, MJ, Trujillo, MA, Davydova, J, McDonough, S, Yamamoto, M, and Morris, JC, 3rd (2013). Effect of increased viral replication and infectivity enhancement on radioiodide uptake and oncolytic activity of adenovirus vectors expressing the sodium iodide symporter. *Cancer gene therapy* **20**: 195-200.

27. Trujillo, MA, Oneal, MJ, McDonough, S, Qin, R, and Morris, JC (2012). A steep radioiodine dose response scalable to humans in sodium-iodide symporter (NIS)-mediated radiovirotherapy for prostate cancer. *Cancer gene therapy* **19**: 839-844.

28. Trujillo, MA, Oneal, MJ, McDonough, SJ, and Morris, JC (2013). Viral dose, radioiodide uptake, and delayed efflux in adenovirus-mediated NIS radiovirotherapy correlates with treatment efficacy. *Gene therapy* **20**: 567-574.

29. Pack, DW, Hoffman, AS, Pun, S, and Stayton, PS (2005). Design and development of polymers for gene delivery. *Nat Rev Drug Discov* **4**: 581-593.

30. Hanahan, D, and Weinberg, RA (2011). Hallmarks of cancer: the next generation. *Cell* **144**: 646-674.

31. Blumenschein, GR, Jr., Mills, GB, and Gonzalez-Angulo, AM (2012). Targeting the hepatocyte growth factor-cMET axis in cancer therapy. *Journal of clinical oncology : official journal of the American Society of Clinical Oncology* **30**: 3287-3296.

32. Broda, E, Mickler, FM, Lachelt, U, Morys, S, Wagner, E, and Brauchle, C (2015). Assessing potential peptide targeting ligands by quantification of cellular adhesion of model nanoparticles under flow conditions. *Journal of controlled release : official journal of the Controlled Release Society* **213**: 79-85.

33. Kim, EM, Park, EH, Cheong, SJ, Lee, CM, Jeong, HJ, Kim, DW, *et al.* (2009). In vivo imaging of mesenchymal-epithelial transition factor (c-Met) expression using an optical imaging system. *Bioconjugate chemistry* **20**: 1299-1306.

34. Kim, EM, Park, EH, Cheong, SJ, Lee, CM, Kim, DW, Jeong, HJ, *et al.* (2009). Characterization, biodistribution and small-animal SPECT of I-125-labeled c-Met binding peptide in mice bearing c-Met receptor tyrosine kinase-positive tumor xenografts. *Nuclear medicine and biology* **36**: 371-378.

35. Rosland, GV, and Engelsen, AS (2015). Novel points of attack for targeted cancer therapy. *Basic & clinical pharmacology & toxicology* **116**: 9-18.

36. Ortiz, R, Melguizo, C, Prados, J, Alvarez, PJ, Caba, O, Rodriguez-Serrano, F, *et al.* (2012). New gene therapy strategies for cancer treatment: a review of recent patents. *Recent patents on anti-cancer drug discovery* **7**: 297-312.

37. Spitzweg, C, Dietz, AB, O'Connor, MK, Bergert, ER, Tindall, DJ, Young, CY, *et al.* (2001). In vivo sodium iodide symporter gene therapy of prostate cancer. *Gene Ther* **8**: 1524-1531.

38. Merron, A, Peerlinck, I, Martin-Duque, P, Burnet, J, Quintanilla, M, Mather, S, *et al.* (2007). SPECT/CT imaging of oncolytic adenovirus propagation in tumours in vivo using the Na/I symporter as a reporter gene. *Gene therapy* **14**: 1731-1738.

39. Groot-Wassink, T, Aboagye, EO, Glaser, M, Lemoine, NR, and Vassaux, G (2002). Adenovirus biodistribution and noninvasive imaging of gene expression in vivo by positron emission tomography using human sodium/iodide symporter as reporter gene. *Human gene therapy* **13**: 1723-1735.

40. Penheiter, AR, Wegman, TR, Classic, KL, Dingli, D, Bender, CE, Russell, SJ, *et al.* (2010). Sodium iodide symporter (NIS)-mediated radiovirotherapy for pancreatic cancer. *AJR American journal of roentgenology* **195**: 341-349.

41.   Barton, KN, Stricker, H, Elshaikh, MA, Pegg, J, Cheng, J, Zhang, Y, *et al.* (2011). Feasibility of adenovirus-mediated hNIS gene transfer and 131I radioiodine therapy as a definitive treatment for localized prostate cancer. *Molecular therapy : the journal of the American Society of Gene Therapy* **19**: 1353-1359.

42.   Dwyer, RM, Schatz, SM, Bergert, ER, Myers, RM, Harvey, ME, Classic, KL, *et al.* (2005). A preclinical large animal model of adenovirus-mediated expression of the sodium-iodide symporter for radioiodide imaging and therapy of locally recurrent prostate cancer. *Molecular therapy : the journal of the American Society of Gene Therapy* **12**: 835-841.

43.   Russell, SJ, Federspiel, MJ, Peng, KW, Tong, C, Dingli, D, Morice, WG, *et al.* (2014). Remission of disseminated cancer after systemic oncolytic virotherapy. *Mayo Clinic proceedings* **89**: 926-933.

44.   Galanis, E, Atherton, PJ, Maurer, MJ, Knutson, KL, Dowdy, SC, Cliby, WA, *et al.* (2015). Oncolytic measles virus expressing the sodium iodide symporter to treat drug-resistant ovarian cancer. *Cancer research* **75**: 22-30.

45.   Peerlinck, I, Merron, A, Baril, P, Conchon, S, Martin-Duque, P, Hindorf, C, *et al.* (2009). Targeted radionuclide therapy using a Wnt-targeted replicating adenovirus encoding the Na/I symporter. *Clinical cancer research : an official journal of the American Association for Cancer Research* **15**: 6595-6601.

46.   Merron, A, Baril, P, Martin-Duque, P, de la Vieja, A, Tran, L, Briat, A, *et al.* (2010). Assessment of the Na/I symporter as a reporter gene to visualize oncolytic adenovirus propagation in peritoneal tumours. *European journal of nuclear medicine and molecular imaging* **37**: 1377-1385.

47.   Penheiter, AR, Dingli, D, Bender, CE, Russell, SJ, and Carlson, SK (2012). Monitoring the initial delivery of an oncolytic measles virus encoding the human sodium iodide symporter to

solid tumors using contrast-enhanced computed tomography. *The journal of gene medicine* **14**: 590-597.

48. Lachelt, U, and Wagner, E (2015). Nucleic Acid Therapeutics Using Polyplexes: A Journey of 50 Years (and Beyond). *Chemical reviews* **115**: 11043-11078.

49. Wang, T, Upponi, JR, and Torchilin, VP (2012). Design of multifunctional non-viral gene vectors to overcome physiological barriers: dilemmas and strategies. *International journal of pharmaceutics* **427**: 3-20.

50. Willhauck, M, Samani, B-R, Wolf, I, Senekowitsch-Schmidtke, R, Stark, H-J, Meyer, G, *et al.* (2008). The potential of 211Astatine for NIS-mediated radionuclide therapy in prostate cancer. *European journal of nuclear medicine and molecular imaging* **35**: 1272-1281.

51. Willhauck, M, Sharif-Samani, B, Senekowitsch-Schmidtke, R, Wunderlich, N, Göke, B, Morris, J, *et al.* (2008). Functional sodium iodide symporter expression in breast cancer xenografts in vivo after systemic treatment with retinoic acid and dexamethasone. *Breast Cancer Research and Treatment* **109**: 263-272.

52. Willhauck, MJ, Sharif Samani, BR, Klutz, K, Cengic, N, Wolf, I, Mohr, L, *et al.* (2008). Alpha-fetoprotein promoter-targeted sodium iodide symporter gene therapy of hepatocellular carcinoma. *Gene therapy* **15**: 214-223.

53. Ediriwickrema, A, and Saltzman, WM (2015). Nanotherapy for Cancer: Targeting and Multifunctionality in the Future of Cancer Therapies. *ACS biomaterials science & engineering* **1**: 64-78.

54. Iyer, AK, Khaled, G, Fang, J, and Maeda, H (2006). Exploiting the enhanced permeability and retention effect for tumor targeting **11**: 812-818.

55. Schaffert, D, Badgujar, N, and Wagner, E (2011). Novel Fmoc-polyamino acids for solid-phase synthesis of defined polyamidoamines. *Organic letters* **13**: 1586-1589.

56. Lachelt, U, Kos, P, Mickler, FM, Herrmann, A, Salcher, EE, Rodl, W, *et al.* (2014). Fine-tuning of proton sponges by precise diaminoethanes and histidines in pDNA polyplexes. *Nanomedicine : nanotechnology, biology, and medicine* **10**: 35-44.

57. Smrekar, B, Wightman, L, Wolschek, MF, Lichtenberger, C, Ruzicka, R, Ogris, M, *et al.* (2003). Tissue-dependent factors affect gene delivery to tumors in vivo **10**: 1079-1088.

58. Zhou, Y, and Kopecek, J (2013). Biological rationale for the design of polymeric anti-cancer nanomedicines. *Journal of drug targeting* **21**: 1-26.

59. USFDA (2005). Guidance for Industry: Estimating the Maximum Safe Starting Dose in Adult Healthy Volunteer. *US Food and Drug Administration*: Rockville.

60. Van Nostrand, D, Atkins, F, Yeganeh, F, Acio, E, Bursaw, R, and Wartofsky, L (2002). Dosimetrically determined doses of radioiodine for the treatment of metastatic thyroid carcinoma. *Thyroid : official journal of the American Thyroid Association* **12**: 121-134.

61. Jo, M, Stolz, DB, Esplen, JE, Dorko, K, Michalopoulos, GK, and Strom, SC (2000). Cross-talk between epidermal growth factor receptor and c-Met signal pathways in transformed cells. *The Journal of biological chemistry* **275**: 8806-8811.

62. Puri, N, and Salgia, R (2008). Synergism of EGFR and c-Met pathways, cross-talk and inhibition, in non-small cell lung cancer. *Journal of carcinogenesis* **7**: 9.

63. Zhang, YW, Staal, B, Essenburg, C, Lewis, S, Kaufman, D, and Vande Woude, GF (2013). Strengthening context-dependent anticancer effects on non-small cell lung carcinoma by inhibition of both MET and EGFR. *Molecular cancer therapeutics* **12**: 1429-1441.

64. Van Der Steen, N, Pauwels, P, Gil-Bazo, I, Castanon, E, Raez, L, Cappuzzo, F, *et al.* (2015). cMET in NSCLC: Can We Cut off the Head of the Hydra? From the Pathway to the Resistance. *Cancers* **7**: 556-573.

65. Spitzweg, C, Baker, CH, Bergert, ER, O'Connor, MK, and Morris, JC (2007). Image-guided radioiodide therapy of medullary thyroid cancer after carcinoembryonic antigen promoter-targeted sodium iodide symporter gene expression. *Human gene therapy* **18**: 916-924.

FIGURE LEGENDS

Figure 1 *cMET/HGFR-targeted NIS gene transfer in vitro*

Surface expression of cMET/HGFR on HuH7 (**a**) and Hep3B cells (**b**) was analyzed by flow cytometry with an antibody that specifically detects human cMET/HGFR and compared to isotype controls. ^{125}I uptake levels were measured in HuH7 and Hep3B cells after i*n vitro* transduction with cMBP2-PEG-Stp/NIS polyplexes (n=3) at an N/P ratio of 12 and results correlated well with cMET/HGFR expression levels (**c**). Further, to identify receptor specificity and NIS-dependency of iodide uptake, HuH7 cells were transfected with untargeted polyplexes Ala-PEG-Stp/NIS (n=3), cMBP2-PEG-Stp/Antisense-NIS (n=3) and polymer without DNA (n=3) (*$p<0.05$; **$p<0.01$) (**d**). Cell viability was not affected by polyplex-mediated gene transfer, as determined by MTT assay (n=3) (**f**). Results are reported as mean ± SEM.

Figure 2 *In vivo and ex vivo iodide uptake studies*

48 h after polyplex administration, vector biodistribution in mice bearing subcutaneous HuH7 xenografts was analyzed by ^{123}I-scintigraphy. Tumoral iodide uptake of cMBP2-PEG-Stp/NIS-treated mice (n=9) (**a**), Ala-PEG-Stp/NIS-treated mice, where the targeting ligand was replaced by alanine (n=5) (**b**), and cMBP2-PEG-Stp/Antisense-NIS treated mice (n=5) (**c**) was measured 3 h post radioiodide injection. A subset of cMBP2-PEG-Stp/NIS-treated mice was pretreated with the NIS-specific inhibitor perchlorate 30 min before ^{123}I application (n=6) (**d**). Iodide accumulation in tumors over the time and the biological half-life of ^{123}I were monitored by serial scanning (**e**). *Ex vivo* biodistribution was performed 3 h after injection of the radionuclide. Organs of cMBP2-PEG-Stp/NIS-treated mice without (n=6) and with sodium-perchlorate-pretreatment (n=3), Ala-PEG-Stp/NIS-treated mice (n=3) and cMBP2-PEG-Stp/Antisense-NIS-treated mice (n=3) were dissected and ^{123}I accumulation in single organs was measured by gamma-counting (**f**). Results are reported as mean ± SEM.

Figure 3 *Analysis of NIS mRNA expression in HuH7 tumors*

NIS protein expression in HuH7 xenografts was analyzed by immunohistochemistry 48 h after cMET-targeted polyplex-mediated gene transfer on frozen tumor section from mice that received cMBP2-Stp-PEG/NIS (**a, b**), from mice that received control polyplexes (Ala-PEG-Stp/NIS (**c**), cMBP2-PEG-Stp/Antisense-NIS (**d**)) and from untreated mice (**e**). Scale bar=100 µm.

Tumoral NIS mRNA expression levels after application of cMBP2-PEG-Stp/NIS with and without sodium-perchlorate-pretreatment, Ala-PEG-Stp/NIS and cMBP2-PEG-Stp/Antisense-NIS were examined by qPCR (**f**).

Figure 4 *In vivo therapeutic efficacy*

The cycle of intravenous gene transfer and radioiodide application was conducted three times on day 0/2, 3/5 and 7/9. Mice were treated either with cMBP2-PEG-Stp/NIS and 55.5 MBq [131]I (n=10), cMBP2-PEG-Stp/NIS followed by application of NaCl (n=9), Ala-PEG-Stp/NIS+[131]I (n=6) or cMBP2-PEG-Stp/Antisense-NIS+[131]I (n=6). Tumor volumes (**a**) and animal survival (Kaplan-Meier-Plot (**p<0.01)) (**b**) of the different therapy groups were compared. Results are either reported as mean ± SEM for tumor volumes or in percent for survival plots.

Figure 5 *Immunofluorescence analysis*

After treatment, when tumors reached a size of 1500mm^3, mice were sacrificed and tumors dissected. Frozen sections of tumor tissue were stained with a Ki67-specific antibody (green) to determine cell proliferation and an antibody against CD31 (red) to label blood vessels (**a-d**). Tumor cell proliferation (**e**) and blood vessel density (**f**) in tumors from animals treated with cMBP2-PEG-Stp/NIS that received [131]I (n=10) were compared to control groups treated with cMBP2-PEG-Stp/NIS+NaCl (n=8), Ala-PEG-

Stp/NIS+^{131}I (n=6) or cMBP2-PEG-Stp/Antisense-NIS+^{131}I (n=6). Nuclei were counterstained with Hoechst. Results are reported as mean ± SEM. Scale bar=100 μm
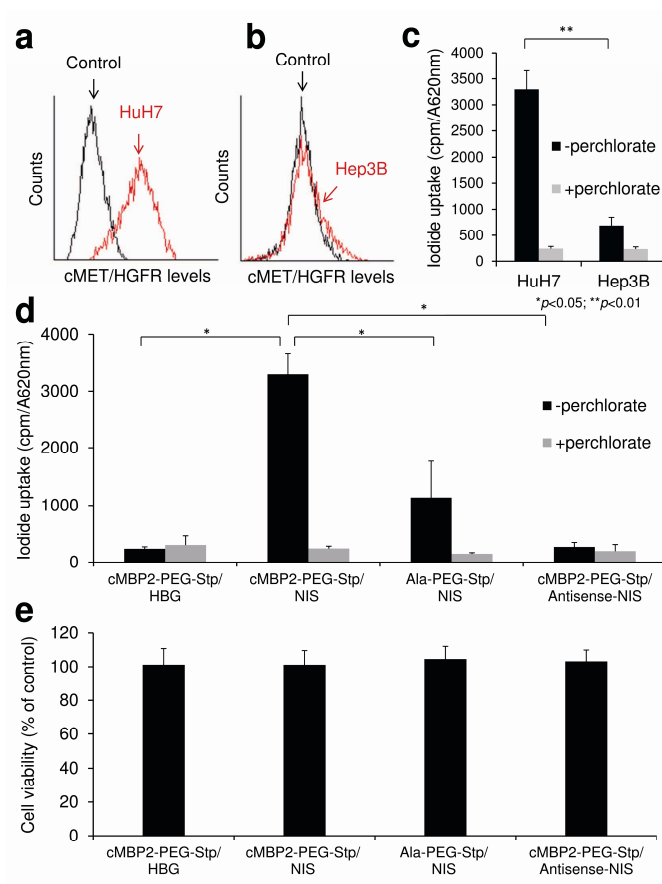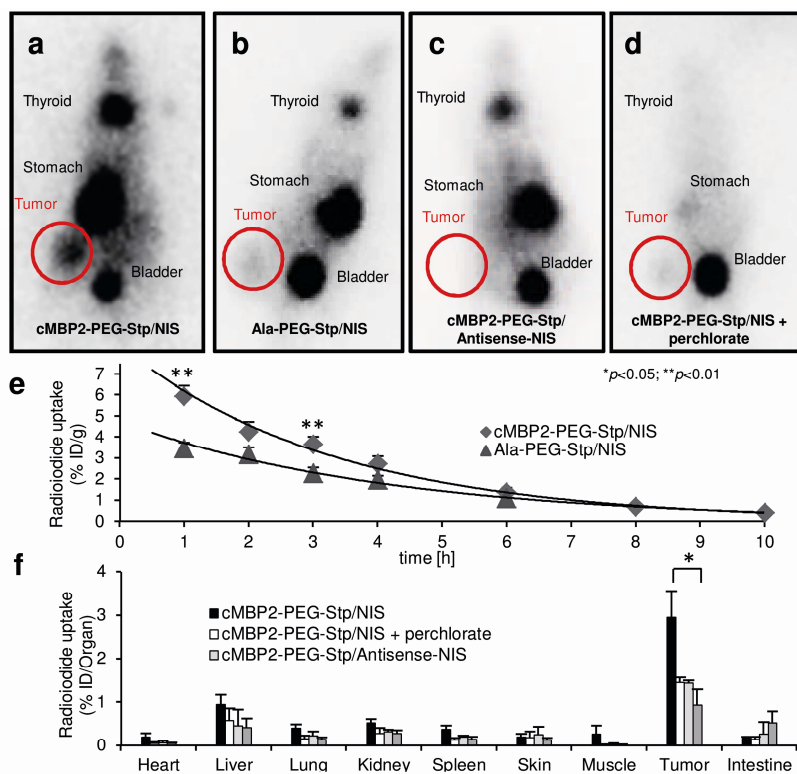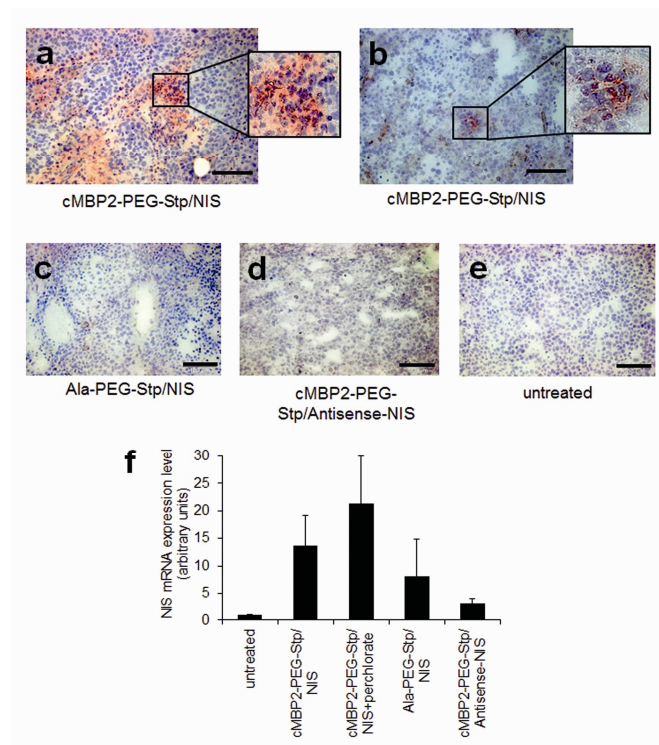
Figure 1

Figure 2

Figure 3

a

cMBP2-PEG-Stp/NIS

b

cMBP2-PEG-Stp/NIS

c

Ala-PEG-Stp/NIS

d

cMBP2-PEG-
Stp/Antisense-NIS

e

untreated

f

Figure 4

a

b

*p<0.05; **p<0.01

Figure 5